

Crystallization behavior of isotactic polypropylene/magnesium salt whisker composites modified by compatibilizer PP-g-MAH

Zhiyong Wei · Wanxi Zhang · Guangyi Chen ·
Jicai Liang · Ying Chang · Lian Liu ·
Pei Wang · Juncai Sun

Received: 19 April 2010/Accepted: 5 July 2010/Published online: 20 July 2010
© Akadémiai Kiadó, Budapest, Hungary 2010

Abstract Crystallization behavior of isotactic polypropylene (iPP)/magnesium salt whisker (MSW) composites modified by compatibilizer PP-g-MAH was studied under both isothermal and nonisothermal conditions. Analysis of the isothermal crystallization showed that the Avrami model successfully described the crystallization process. On the basis of Lauritzen–Hoffman theory, a regime transition was observed at about 139 °C for the iPP/MSW composite, and a decrease in the fold surface free energy was calculated with the addition of MSW and PP-g-MAH. The addition of MSW filler and PP-g-MAH compatibilizer distinctly improved the crystallization temperature and accelerated the total crystallization rate of iPP. It was observed that MSW induced the formation of β -iPP but PP-g-MAH suppressed the formation of β -iPP.

Keywords Crystallization · Isotactic polypropylene · Magnesium salt whisker · Melting behavior

Introduction

Isotactic polypropylene (iPP), as one of the widely used commodity plastics, has been of practical use in many areas like packaging, households, and automotives, because of its well balanced physical and mechanical

properties, as well as to easy processing at a relatively low cost. The application of iPP, however, has been limited by its high flammability, tendency to brittleness at temperatures below its glass transition temperature, and low stiffness particularly at elevated temperatures.

As one-dimensional functional materials, whiskers have attracted great attention because they exhibit unique structure and various excellent physical, chemical, and mechanical properties, which are distinctive from those of conventional bulk materials [1, 2]. Because the whiskers are short, fiber-shaped single crystals with high tensile strength owing to their nearly perfect microstructure [3], they have undoubtedly been of great interest for many researchers. Among the various whiskers, the magnesium salt whisker (MSW), with a molecular formula $MgSO_4 \cdot 5Mg(OH)_2 \cdot 3H_2O$, is a new promising class of whiskers [4, 5]. It is not only used as a potential reinforcement of polymers, but also as a good flame retardant. Hence, incorporation of MSW is an effective way to improve the thermal and mechanical properties of the filled polymers [6–10]. Lu investigated the fire properties of low density polyethylene (LDPE) composites filled with MSW and microencapsulated red phosphor and reported that the two flame retardant additives have a synergic effect of flame retardance in the LDPE/MSW composites [6, 7]. Liu researched the effects of MSW on the flame retardant ABS composites and concluded that the MSW content had great influence on the flame retardancy and rheological behavior of composites [8]. Ouyang found that the MSWs are good reinforcements for ABS and the surface treatment of the whiskers also strongly affected the mechanical properties of the composites [9].

It is well recognized that some inorganic filler, as a reinforcing agent in composites, can induce nucleation for crystallization and accelerated overall crystallization process [11–14]. In general, mineral fillers can influence the

Z. Wei (✉) · W. Zhang · G. Chen · J. Liang · Y. Chang
School of Automotive Engineering, Dalian University of
Technology, Dalian 116024, China
e-mail: zywei@dlut.edu.cn

L. Liu · P. Wang · J. Sun
School of Transportation and Logistics Engineering, Dalian
Maritime University, Dalian 116026, China

crystallization process of the polymer matrix by acting as heterogeneous nuclei. The heterogeneous nucleation leads to the increase in nucleation and crystallization rate. The interfacial adhesion can also influence the crystalline of iPP in filler-filled polymer composites [15–17]. Owing to the low polarity of iPP, it is usually necessary to use polar compatibilizers to promote strong interactions between the polymer melt and the fillers. The improvement of the interfacial adhesion between polymer and filler can reduce the free energy of a nucleation process, which is favorable to nucleation process at the phase boundary [18–20].

Furthermore, the final physical and mechanical properties of crystalline polymers like iPP depend on the morphology, crystalline structure, and degree of crystallization [21, 22]. In their processing, the fillers in polymeric-based composites act as a nucleating agent and, thus, affect the crystallization behavior of polymer matrix. Therefore, the knowledge of the crystallization kinetics is necessary for optimizing industrial process, conditions, and establishing the structure–property correlations in the case of the filled polymer-based composites [23–25].

As far as we know, no study about the effect of MSW on the crystallization behavior of iPP has been published. In this study, iPP/MSW composites were prepared by melt mixing using PP-g-MAH as a compatibilizer. The purpose of this article was to investigate the effects of MSW filler and PP-g-MAH compatibilizer on crystallization and melting behavior of iPP matrix in PP/MSW composites.

Experimental

Materials

Isotactic polypropylene (iPP) was T30S with isotacticity index of 95% and melt flow index (MFI) of 2.5 g/10 min (230 °C/2.16 kg), supplied by West Pacific Petrochemical (Dalian, China). MSWs used in this study were produced by Yingkou Whiskers Chemicals Co. Ltd. (Yingkou China). The characteristics of the needle-shaped whisker are given as follows: the average length ranges from 10 to 60 μm, the diameter 0.5–1 μm, and the length/diameter ratio >30. Polypropylene grafted with maleic anhydride (PP-g-MAH, MFI > 15 g/10 min at 230 °C/2.16 kg, MAH grafting ratio = 1 mass%) was used as compatibilizer, which was supplied by Nanjing Deba Chemical Co. (Nanjing, China).

Sample preparation

The iPP/MSW/PP-g-MAH composites were prepared by melt mixing all the components in a one-step procedure

using a HAAKE (Thermo Haake Rheomix) twin-screw extruder ($L/D = 40$, $D = 12.5$ mm). The blending temperature profile is 190/180/190/190/200/190/180 °C. The compositions for the different iPP/MSW/PP-g-MAH composites used in this study were 100/0/0, 80/20/0, 76/20/4, and the three samples were denoted as iPP, iPP/MSW, and iPP/MSW/PP-g-MAH, respectively.

DSC measurements

Isothermal and nonisothermal crystallizations were performed in a DSC1 (Mettler-Toledo, Switzerland) differential scanning calorimeter. The instrument was calibrated using high purity indium and zinc standards. Each sample (ca. 2–3 mg) was initially melted at 200 °C for 5 min to erase the previous thermal history, then cooled rapidly to the predetermined crystallization temperature (T_c), and maintained until the crystallization of the matrix was completed. For nonisothermal crystallization, after melting at 200 °C for 5 min, the sample was cooled to 80 °C at various cooling rates of 5, 10, 15, 20, and 30 °C min⁻¹. After the completion of crystallization, the sample was subsequently heated to 200 °C at 10 °C min⁻¹. The heat flow during both crystallization and melting process was recorded.

Results and discussion

Isothermal crystallization behavior

Isothermal crystallization of iPP/MSW composites was performed at various temperature ranges. DSC crystallization exotherms for pure iPP, iPP/MSW, and iPP/MSW/PP-g-MAH composites are shown in Fig. 1. The higher the T_c is, the slower the crystallization process is. It is evident that the crystallization rate of iPP can be enhanced greatly by adding MSW filler and PP-g-MAH compatibilizer. Using approximate crystallization time, the isothermal crystallization temperature (T_c) interval of iPP was between 123 and 129 °C, and those of iPP/MSW and iPP/MSW/PP-g-MAH composites shifted to higher T_c s 136–142 and 141–147 °C, respectively. These shifts revealed that MSW is an effective nucleating agent during the course of isothermal crystallization of iPP, and PP-g-MAH compatibilizer further enhanced the nucleation activity of MSW on iPP by its improved interaction between MSW and iPP.

In order to further analyze the isothermal crystallization process, the crystallization kinetics of iPP and iPP/MSW composites is compared. Based on the assumption that the evolution of crystallinity is linearly proportional to the evolution of heat released during the crystallization, the

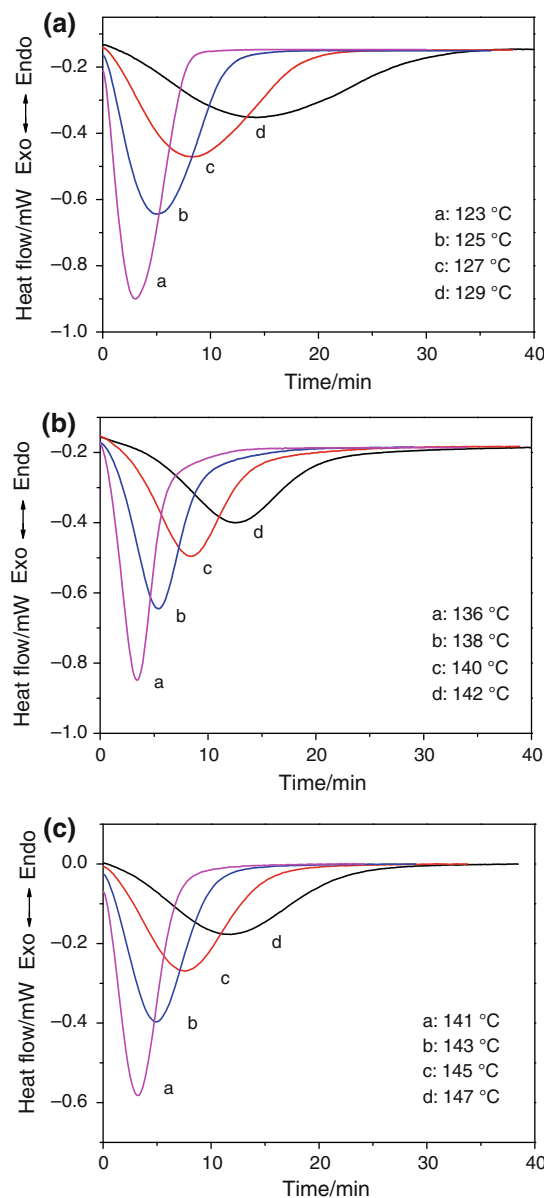


Fig. 1 DSC thermograms of isothermal crystallization of **a** iPP, **b** iPP/MSW, and **c** iPP/MSW/PP-g-MAH composites at various temperatures

relative degree of crystallinity, X_t , can be calculated by integration of the exothermal peaks from the following equation:

$$X_t = \frac{X_t(t)}{X_t(\infty)} = \frac{\int_0^t (dH_c/dt)dt}{\int_0^\infty (dH_c/dt)dt} \quad (1)$$

where dH_c/dt denotes the rate of heat flow, $X_t(t)$ and $X_t(\infty)$ represent the absolute crystallinity at the elapsed time during the course of crystallization and at the end of the crystallization process, respectively.

As shown in Fig. 2, the evolution of relative crystallinity with crystallization time at various temperatures shows the

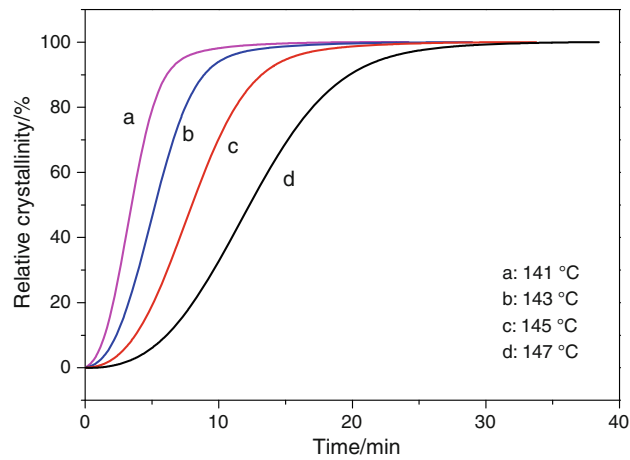


Fig. 2 Relative crystallinity as a function of time for isothermal crystallization of iPP/MSW/PP-g-MAH composite

Table 1 Results of the Avrami analysis for isothermal crystallization of iPP and iPP/MSW composites

Sample	$T_c/^\circ\text{C}$	n	Z_t/min^{-n}	$t_{1/2}/\text{min}$	n (average)
iPP	123	2.14	0.0498	3.5	2.27
	125	2.29	0.0130	5.7	
	127	2.27	0.0048	8.9	
	129	2.36	0.0012	14.7	
iPP/MSW	136	2.56	0.0279	3.5	2.75
	138	2.55	0.0105	5.2	
	140	2.88	0.0013	8.7	
	142	3.02	0.0003	12.7	
iPP/MSW/PP-g-MAH	141	2.16	0.0470	3.5	2.34
	143	2.31	0.0150	5.1	
	145	2.46	0.0041	8.0	
	147	2.44	0.0017	12.3	

similar S-shaped curves, which are consistent with nucleation and growth processes. The half time of crystallization at 50% crystallization ($t_{1/2}$) obtained from these curves is frequently used to evaluate the rate of crystallization of iPP. The shorter the $t_{1/2}$ is, the higher the crystallization rate is. The obtained $t_{1/2}$ values for iPP and its composites are summarized in Table 1. It is apparent that the values of $t_{1/2}$ increase with increasing crystallization temperature.

The so-called Avrami method is the most common approach to analyze the isothermal crystallization [26–28]. Accordingly, the relative degree of crystallinity, X_t , is related to the crystallization time, t , according to:

$$X_t = 1 - \exp(-Z_t t^n) \quad (2)$$

$$\ln[-\ln(1 - X_t)] = \ln Z_t + n \ln t \quad (3)$$

where n is the Avrami exponent, which is relevant to the mechanism of nucleation, and it contains information on nucleation and growth geometry, and Z_t is the overall

crystallization rate constant, which is dependent on nucleation and crystal growth.

The representative Avrami plots for iPP/MSW/PP-g-MAH composite obtained at various temperatures are illustrated in Fig. 3. In these plots, an initial linear part in a wide relative crystallinity range is observed, which was used for the estimation of the parameters n and Z_r . The deviation after this first linear part is often attributed to secondary crystallization. From the slope and the intercept of the Avrami plots, values of n and Z_r , respectively, were calculated and summarized in Table 1. The values of n obtained for pure iPP and iPP/MSW composites were in the vicinity of 2.5 ± 0.25 , and they should possibly be related with heterogeneous nucleation. The results indicated that the addition of MSW with/without PP-g-MAH has not greatly altered the dimension of iPP crystalline growth.

Lauritzen–Hoffman Analysis

The crystallization thermodynamics and kinetics of the iPP/MSW composites have been analyzed on the basis of the theory of Lauritzen–Hoffman [29, 30]. Accordingly, the spherulite growth rate (G) is given as a function of the crystallization temperature (T_c) by the following bi-exponential equation:

$$G = G_0 \exp\left[-\frac{U^*}{R(T_c - T_\infty)}\right] \exp\left[-\frac{K_g}{T_c \Delta Tf}\right] \quad (4)$$

where G_0 is the pre-exponential factor, the first exponential term contains the contribution of the diffusion process to the growth rate, while the second exponential term is the contribution of the nucleation process. U^* denotes the activation energy that characterizes molecular diffusion across the interfacial boundary between melt and crystals,

and the universal value for U^* is $6270 \text{ Jmol}^{-1} K_g$ is a nucleation constant and ΔT denotes the degree of undercooling ($\Delta T = T_m^o - T_c$). T_∞ is the temperature below which diffusion stops, $T_\infty = T_g - 30 \text{ K}$. In this study, the T_g value of iPP used is 263 K and T_m^o is 481 K . f is a correcting factor for variation in the heat of fusion with temperature and it is defined as $f = 2T_c/(T_m^o + T_c)$ [31].

Instead of using Polarized light optical microscopy (POM) measurements, several authors have treated the isothermal crystallization rate data obtained by DSC according to the Lauritzen–Hoffmann analysis [Eq. (4)] [24, 32–34]. The basic assumption used for the evaluation of G was that the spherulite growth rate is inversely proportional to the crystallization half time, i.e. $G \approx 1/t_{1/2}$ [32]. This approximation, although it is purely empirical, has been widely used in the literature [33, 34]. Accordingly, Eq. (4) is rewritten as:

$$\ln\left(\frac{1}{t_{1/2}}\right) + \frac{U^*}{R(T_c - T_\infty)} = B - \frac{K_g}{T_c \Delta Tf} \quad (5)$$

In this study, more wide crystallization temperature ranges tested in isothermal crystallizations were used for the evaluation of nucleation constant (K_g). Figure 4 shows that the values of $t_{1/2}$ strongly depend on the crystallization temperature (T_c) and increase almost exponentially as the crystallization temperature is increased.

As shown in Fig. 5, plotting the left hand side of Eq. (5) with respect to $1/T_c \Delta Tf$ a straight line should appear a slope equal to $-K_g$. Critical break points, identified by the change in the slope of the line, when appear in such a plot, have been attributed to regime transitions accompanied by morphological changes of the crystals formed (i.e., change from axialite-like to banded spherulite and non-banded spherulite morphology). In the case of pure iPP, there are two regimes with different slopes, indicating that pure iPP has a

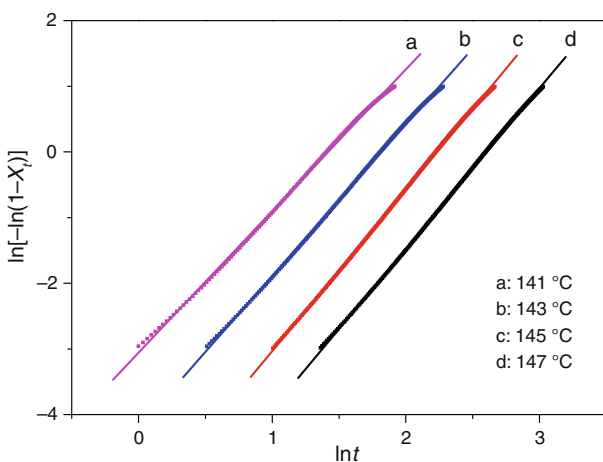


Fig. 3 Avrami plots of $\ln[-\ln(1-X_t)]$ versus Int for isothermal crystallization of iPP/MSW/PP-g-MAH composite

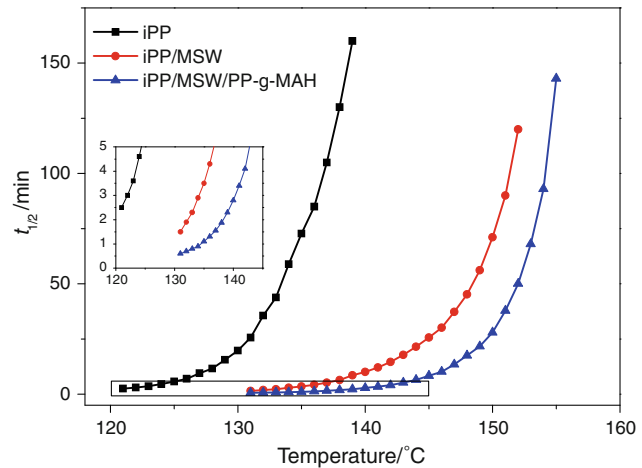


Fig. 4 Dependence of $t_{1/2}$ on crystallization temperature (T_c) for iPP and iPP/MSW composites

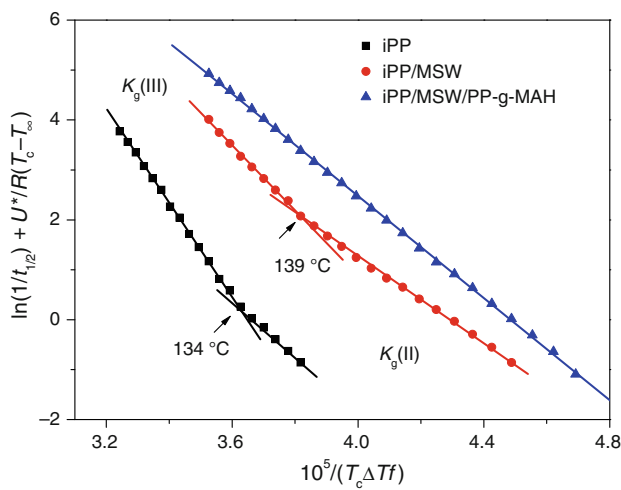


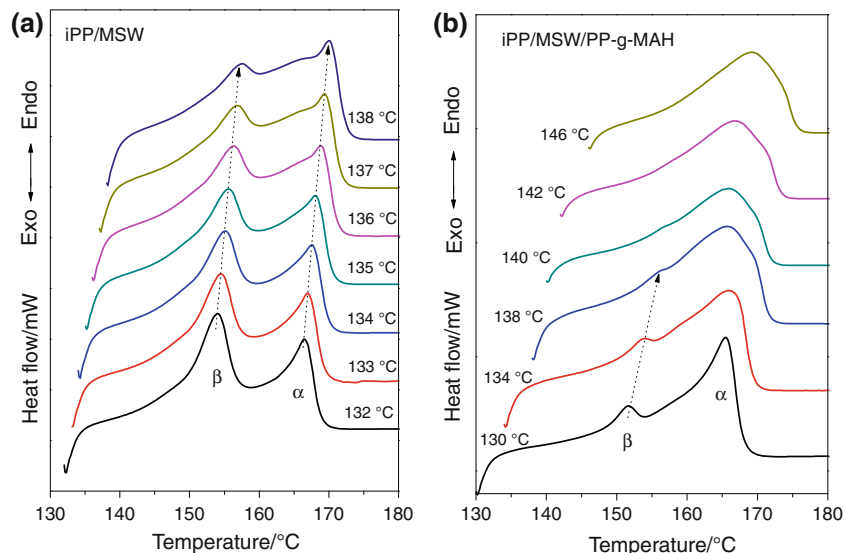
Fig. 5 Plots of $\ln(1/t_{1/2}) + U^*/R(T_c - T_\infty)$ versus $10^5/(T_c \Delta Tf)$ for iPP and iPP/MSW composites

Table 2 Nucleation parameter of iPP and iPP/MSW composites obtained using Lauritzen–Hoffmann equation

Sample	$K_g/10^5\text{K}^2$	σ_e/Jm^{-2}	Regime	$K_g(\text{III})/K_g(\text{II})$
iPP	9.26	0.153	III	1.60
	5.78	0.192	II	
iPP/MSW	7.44	0.123	III	1.73
	4.32	0.143	II	
iPP/MSW/PP-g-MAH	5.11	0.085	III	

transition from regime II to regime III occurring at approximately 134 °C, which is close to the reported values of about 135–138 °C [35]. The transition from regime III to regime II for the iPP/MSW composite shifted to a high temperature at 139 °C. However, such a regime transition was not observed for the iPP/MSW/PP-g-MAH composite.

Fig. 6 Melting curves of **a** iPP/MSW and **b** iPP/MSW/PP-g-MAH composites isothermally crystallized at various temperatures as indicated



The obtained results are summarized in Table 2. As it can be seen all data for every sample follow the straight line with a regression coefficient 0.999. The ratios of $K_g(\text{III})/K_g(\text{II})$ were about 1.6–1.7, close to the theoretically value 2.0 predicted by Lauritzen–Hoffman theory.

For a secondary or heterogeneous nucleation, K_g can be calculated from:

$$K_g = \frac{n_A \sigma \sigma_e b_o T_m^0}{k \Delta H} \quad (6)$$

where n_A is the variable that considers the crystallization regime and assumes the value $n_A = 4$ for regimes I and III and $n_A = 2$ for regime II [36]. k is the Boltzmann constant, b_o the thickness of the molecular layer determined by lattice parameters, ΔH is the theoretical heat of fusion, and σ and σ_e are interfacial free energies per unit area parallel and perpendicular to the molecular chain direction, respectively. The value of σ can be calculated from the following expression:

$$\sigma = ab_o \Delta H \quad (7)$$

where a is an empirical constant close to 0.1, b_o is $6.56 \times 10^{-10} \text{ m}$ and ΔH is $1.34 \times 10^8 \text{ Jm}^{-3}$ for pure iPP; then the value of σ for iPP is $8.79 \times 10^{23} \text{ Jm}^{-2}$ [37]. Once the value of K_g was determined, the corresponding fold surface free energy (σ_e) was calculated from Eq. (6) and listed in Table 2.

There is a clear tendency for σ_e to decrease with the addition of MSW filler and PP-g-MAH compatibilizer. As it is well known, a foreign surface frequently reduces the nucleus size needed for crystal growth since the creation of the interface between the polymer crystal and substrate may be less hindered than the creation of the corresponding free polymer crystal surface [17]. The decrease of σ_e could indicate an increase in the entropy of folding and,

therefore, the formation of less homogeneous and regular folding surface. Based on the results of iPP/MSW composites, it is thus verified that the addition of MSWs reduces the work needed to create a new surface, hence leading to faster crystallization rates.

Melting behavior after isothermal crystallization

After completion of isothermal crystallization, the subsequent melting behavior of pure iPP and iPP/MSW composites was measured by DSC at a heating rate of $10\text{ }^{\circ}\text{C min}^{-1}$. Figure 6 presents the melting curves of isothermally crystallized iPP/MSW and iPP/MSW/PP-g-MAH composites at different crystallization temperatures. The melting profile of the samples appears as two melting endotherms, a peak of broad and poorly defined shoulder around $150\text{ }^{\circ}\text{C}$ belong to the melting of β -PP, and another peak of well-defined maximum near to $165\text{ }^{\circ}\text{C}$ is related to the melting of α -PP [18]. It is clearly observed that all the melting peak temperatures shift to higher values with increasing the crystallization temperature (T_c), which is directly related to the perfections of the crystals formed at higher crystallization temperatures (i.e., low undercooling).

The increase in crystallization temperatures of iPP facilitates the formation of α -iPP, but weakens the formation of β -iPP. In the case of iPP/MSW, the ceiling temperature for the formation of β -iPP was observed above $138\text{ }^{\circ}\text{C}$, whereas for the iPP/MSW/PP-g-MAH composite, the critical temperature shifted to a low temperature below $138\text{ }^{\circ}\text{C}$, this indicated that MSW has an effective β -nucleation effect on iPP and PP-g-MAH suppressed the formation of β -iPP.

Nonisothermal crystallization behavior

From dynamic crystallization experiments, data for the crystallization exotherms as a function of temperature, dH_c/dT can be obtained, for each cooling rate, as one can see in Fig. 7 for the crystallization exotherms on cooling of pure iPP, iPP/MSW, and iPP/MSW/PP-g-MAH composites. As expected, with the cooling rate increasing, the crystallization curve shifted to a lower temperature region for each sample.

The relative degree of crystallinity as a function of temperature, $X(T)$, can be formulated as:

$$X(T) = \frac{\int_{T_o}^T (dH_c/dT)dT}{\int_{T_o}^{T_\infty} (dH_c/dT)dT} \quad (9)$$

Where T_o and T_∞ represent the temperatures at the onset and the end of the crystallization process, respectively.

The evolution of the relative crystallinity as a function of temperature at all the different cooling rates gives reversal S-type curves, and it shows a slower process during the later

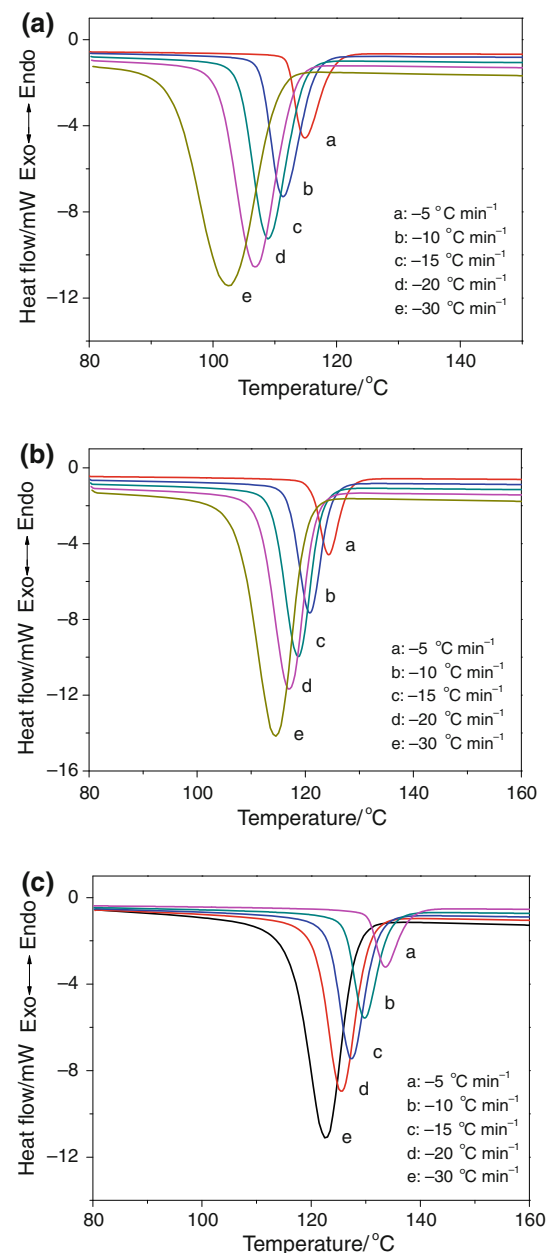


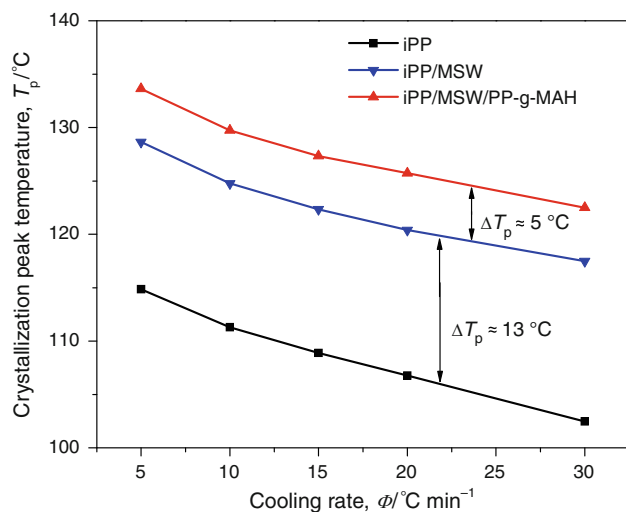
Fig. 7 DSC thermograms of nonisothermal crystallization of **a** iPP, **b** iPP/MSW, and **c** iPP/MSW/PP-g-MAH composites at various cooling rates

crystallization stage. On the basis of these curves, some parameters, including the temperature at 1% relative crystallinity ($T_{0.01}$), the temperature at the maximum crystallization rate (T_p) (i.e., the crystallization peak temperature), and the temperature at 99% relative crystallinity ($T_{0.99}$), can be obtained and summarized in Table 3. It should be noted that $T_{0.01}$ and $T_{0.99}$, respectively, represent the obvious beginning and ending of the crystallization process.

Usually, the addition of inorganic fillers can largely enhance the crystallization rate and the crystallization temperature, due to its heterogeneous nucleation effect. As

Table 3 Kinetics data of nonisothermal crystallization of iPP and iPP/MSW composites

Sample	$\Phi/^\circ\text{C min}^{-1}$	$T_{0.01}/^\circ\text{C}$	$T_p/^\circ\text{C}$	$T_{0.99}/^\circ\text{C}$	$\Delta t_{\text{inc}}^{\text{a}}/\text{min}$	$\Delta t_c^{\text{b}}/\text{min}$	$t_{\text{total}}^{\text{c}}/\text{min}$
iPP	5	121.61	114.85	98.94	15.68	4.53	20.21
	10	118.40	111.30	94.80	8.16	2.36	10.52
	15	116.33	108.88	92.21	5.58	1.61	7.19
	20	114.62	106.76	91.62	4.27	1.15	5.42
	30	111.02	102.47	89.09	2.97	0.73	3.70
iPP/MSW	5	139.94	128.65	106.71	12.01	6.65	18.66
	10	136.27	124.76	104.21	6.37	3.21	9.58
	15	133.84	122.33	103.64	4.41	2.01	6.42
	20	131.63	120.39	102.63	3.42	1.45	4.87
	30	128.23	117.49	100.76	2.39	0.92	3.31
iPP/MSW/PP-g-MAH	5	140.85	133.64	112.61	11.83	5.65	17.48
	10	137.26	129.74	111.58	6.27	2.57	8.84
	15	134.98	127.33	110.53	4.33	1.63	5.96
	20	133.01	125.73	109.77	3.35	1.16	4.51
	30	130.12	122.49	107.96	2.33	0.74	3.07

^a $\Delta t_{\text{inc}} = (200 - T_{0.01})/\Phi$ ^b $\Delta t_c = (T_{0.01} - T_{0.99})/\Phi$ ^c $t_{\text{total}} = \Delta t_{\text{inc}} + \Delta t_c$ **Fig. 8** Crystallization peak temperature (T_p) of iPP and iPP/MSW composites as a function of cooling rate

shown in Fig. 8, a distinct increase of 13 °C in the crystallization peak temperature was achieved by addition of MSW. For iPP/MSW composites modified by PP-g-MAH, a further increase in T_p by 5 °C was observed.

With the following equation, the relative crystallinity can be converted from a function of the crystallization temperature (T) into a function of crystallization time (t):

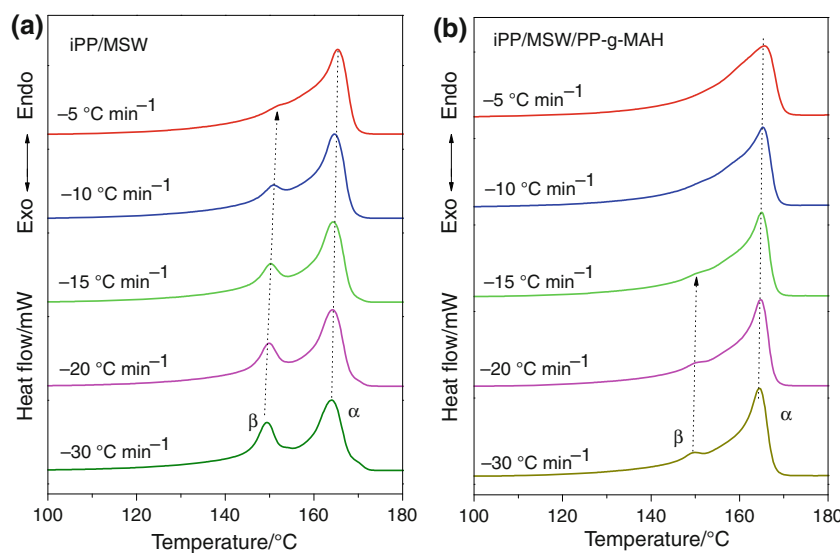
$$t = (T_0 - T)/\Phi \quad (10)$$

where t denotes an arbitrary crystallization time, T_0 denotes the onset temperature of crystallization (i.e., $T_{0.01}$), and Φ denotes the cooling rate.

We must notice here that these time-dependent relative crystallinity $X(t)$ curves do not include the apparent incubation period (Δt_{inc}), defined as the time that a polymer sample spends from the temperature at which it is brought to crystallize (i.e., the initial temperature (T_{ini})) to the onset temperature (i.e., $T_{0.01}$ summarized in Table 3) at which detectable crystallites are observed (i.e., $\Delta t_{\text{inc}} = (T_{\text{ini}} - T_{0.01})/\Phi$, $T_{\text{ini}} = 200$ °C in this study). Some nonisothermal crystallization time parameters, $t_{0.01}$, and $t_{0.99}$, which represent the time at 1% relative crystallinity and at 99% relative crystallinity, respectively, can be obtained. It should be noted that the $t_{0.01}$ and $t_{0.99}$ values are qualitative measurements of the beginning and the ending of the crystallization processes. We define the apparent crystallization period (Δt_c) as the difference between the ending and the beginning of the crystallization process (i.e., $\Delta t_c = (t_{0.99} - t_{0.01}) = (T_{0.01} - T_{0.99})/\Phi$). The apparent total crystallization time (t_{total}) can be calculated directly as $t_{\text{total}} = \Delta t_{\text{inc}} + \Delta t_c$. The values of Δt_{inc} , Δt_c , and t_{total} for various cooling rates are also summarized in Table 3. Clearly, the larger the cooling rate, the shorter the time required for the completion of the crystallization process.

According to the data presented in Table 3, in the case of each given identical cooling rate, the order of the values of the apparent incubation period (Δt_{inc}) is iPP > iPP/MSW > iPP/MSW/PP-g-MAH, which is in accordance with the $T_{0.01}$ values. However, with respect to the apparent crystallization period (Δt_c), the order changes as follows: iPP/MSW > iPP/MSW/PP-g-MAH > iPP. It is well known that the crystallization process can be divided into

Fig. 9 Melting curves of **a** iPP/MSW and **b** iPP/MSW/PP-g-MAH composites after nonisothermal crystallization at various cooling rates as indicated



two steps: nucleation and crystal growth. The total crystallization rate of this process is determined by both the rate of nucleation and the rate of crystal growth. In the case of the composites studied in this study, the overall crystallization process for the samples was mainly controlled by the nucleation step. The above results indicate that nucleation and crystal growth are two independent processes for the composites. As we known, the effect of different kinds of fillers on the spherulite growth rate of iPP varies. Some may retard the spherulite growth. Nitta et al. [38] investigated the effect of silica particles on the spherulite growth rate of iPP and observed that the growth rate decreased with increasing the silica content. Recently, Wang et al. [15, 39] observed that the depressed spherulite growth rate of iPP with the addition of BaSO₄ and explained the reason as the enhanced PP/BaSO₄ interaction promotes the particles to serve as physical crosslinking points. In our study, MSW fillers enhanced the nucleation rate and the total crystallization rate, but a retard of crystal or spherulite growth rate of iPP was observed from the DSC measurements. However, PP-g-MAH accelerated the crystal growth rate at a certain extent. We assumed that the longer whiskers act as an obstacle and baffle the movement of iPP macromolecules segments, and the enhanced iPP/MSW interaction by the compatibilizer promotes their regular arrangements.

Melting behavior after nonisothermal crystallization

Finally, the subsequent melting behavior of iPP/MSW composites after nonisothermal crystallization was studied at a heating rate of 10 °C min⁻¹. The melting curves of iPP/MSW composites are shown in Fig. 9. Besides a large α -melting peak at 165 °C, another distinct peak appears on

the melting curve at lower temperature, which corresponds to the β -phase of iPP. Our experimental results indicated that MSW significantly induced the formation of β -crystals and corroborated the earlier observations about the β -nucleating ability of Mg(OH)₂ fillers [17]. A possible reason for its β -nucleating effect would be connected to the similar Bravais lattice of β -iPP and magnesium compound fillers. And the ionic spacing of the filler crystal lattice is close to the crystallographic dimensions of the polymer crystal, which can support epitaxial polymer crystallization on filler surfaces [17].

When PP-g-MAH was used as compatibilizer, the melting behavior of iPP changed obviously. The β -crystal melting peak near 150 °C in the case of iPP/MSW/PP-g-MAH composite markedly reduced in comparison with iPP/MSW composite. Therefore, we concluded that the PP-g-MAH suppressed the formation of β -iPP. The reason for this can be primarily explained by the α -nucleating effect of PP-g-MAH [18, 40]. Another factor, which may play a significant role in suppressing the formation of the β -modification by PP-g-MAH, is the selective encapsulation of the whiskers by the polar PP-g-MAH phase [18, 41].

The β -melting behavior of iPP/MSW composites is also dependent on the cooling rate. With the decrease of cooling rate, the intensity of the β -melting peak decreased monotonously and the position of the peak shifted to higher temperatures for iPP/MSW composites. At lower cooling rate, there was sufficient time to overcome the nucleation barrier, and so the crystallization started at a higher temperature region. It is well known that a higher crystallization temperature is unfavorable for the formation of β -crystals. It cannot afford enough nuclei to initiate β -crystals, and the β -iPP melting peak almost disappears. And at high cooling rate, the result is reverse.

Conclusions

Effects of MSW filler and PP-g-MAH compatibilizer on the crystallization and melting behavior of iPP were studied by DSC. It is observed that the addition of MSW remarkably affected the crystallization rate and melting behavior of iPP/MSW composites. The addition of MSW and/or PP-g-MAH has strong nucleation activity and accelerates the nucleation rate and the overall crystallization rate. MSW could induce the formation of β -iPP and PP-g-MAH suppresses the formation of β -iPP. At a higher the crystallization temperature or a lower cooling rate, it is unfavorable for the formation of β -crystals, leading to the disappearance of β -iPP melting peak.

Acknowledgements The research was financed by the National High Technology Research and Development Program of China (863 Program No. 2009AA03Z319), and the National Natural Science Foundation of China (No. 50901011), and the Fundamental Research Funds for the Central Universities.

References

- Tjong SC, Meng YZ. Performance of potassium titanate whisker reinforced polyamide-6 composites. *Polymer*. 1998;39:5461–6.
- Tjong SC, Meng YZ. Properties and morphology of polyamide 6 hybrid composites containing potassium titanate whisker and liquid crystalline copolyester. *Polymer*. 1999;40:1109–17.
- Courtney TH. Mechanical behavior of materials. New York: McGraw Hill; 1990.
- Ma PH, Wei ZQ, Xu G, Bao JQ, Wen XM. Dehydration and desulfurization of magnesium oxysulfate whisker. *J Mater Sci Lett*. 2000;19:257–8.
- Xiang L, Liu F, Li J, Jin Y. Hydrothermal formation and characterization of magnesium oxysulfate whiskers. *Mater Chem Phys*. 2004;87:424–9.
- Lu HD, Hu Y, Yang Z, Wang ZZ, Chen ZY, Fan WC. Study of the fire performance of magnesium hydroxide sulfate hydrate whisker flame retardant polyethylene. *Macromol Mater Eng*. 2004;289:984–9.
- Lu HD, Hu Y, Xiao JF, Wang ZZ. Magnesium hydroxide sulfate hydrate whisker flame retardant polyethylene/montmorillonite nanocomposites. *J Mater Sci*. 2006;41:363–7.
- Liu B, Zhang Y, Wan CY, Zhang YX, Li RX, Liu GY. Thermal stability, flame retardancy and rheological behavior of ABS filled with magnesium hydroxide sulfate hydrate whisker. *Polym Bull*. 2007;58:747–55.
- Ouyang YX, Sui GX, Yang R, Zhuang GS. Preparation and mechanical properties of magnesium salt whisker/ABS composites. *Mater Manuf Process*. 2006;21:191–7.
- Fang SL, Hu Y, Song L, Zhan J, He QL. Mechanical properties, fire performance and thermal stability of magnesium hydroxide sulfate hydrate whiskers flame retardant silicone rubber. *J Mater Sci*. 2008;43:1057–62.
- Galeski A. Strength and toughness of crystalline polymer systems. *Prog Polym Sci*. 2003;28:1643–99.
- Chen J-H, Yao B-X, Su W-B, Uang Y-B. Isothermal crystallization behavior of isotactic polypropylene blended with small loading of polyhedral oligomeric silsesquioxane. *Polymer*. 2007;48:1756–69.
- Zhou Z, Cui L, Zhang Y, Zhang Y, Yin N. Isothermal crystallization kinetics of polypropylene/POSS composites. *J Polym Sci Part B Polym Phys*. 2008;46:1762–72.
- Ardanuy M, Velasco JI, Realinho V, Arencón D, Martínez AB. Non-isothermal crystallization kinetics and activity of filler in polypropylene/Mg-Al layered double hydroxide nanocomposites. *Thermochim Acta*. 2008;479:45–52.
- Wang K, Wu J, Zeng H-M. Crystallization and melting behaviour of polypropylene/barium sulfate composites. *Polym Int*. 2004;53:838–43.
- Ning N, Yin Q, Luo F, Zhang Q, Du R, Fu Q. Crystallization behavior and mechanical properties of polypropylene/halloysite composites. *Polymer*. 2007;48:7374–84.
- Naffakh M, Martin Z, Marco C, Gomez MA, Jimenez I. Isothermal crystallization kinetics of isotactic polypropylene with inorganic fullerene-like WS₂ nanoparticles. *Thermochim Acta*. 2008;472:11–6.
- Menyhárd A, Varga J. The effect of compatibilizers on the crystallisation, melting and polymorphic composition of β -nucleated isotactic polypropylene and polyamide 6 blends. *Eur Polym J*. 2006;42:3257–68.
- Shen H, Wang Y, Mai K. Non-isothermal crystallization behavior of PP/Mg(OH)₂ composites modified by different compatibilizers. *Thermochim Acta*. 2007;457:27–34.
- Ning N, Luo F, Wang K, Du R, Zhang Q, Chen F, Fu Q. Interfacial enhancement by shish-calabash crystal structure in polypropylene/inorganic whisker composites. *Polymer*. 2009;50:3851–6.
- Feng D, Caulfield DF, Sanadi AF. Effect of compatibilizer on the structure-property relationships of kenaf-fiber/polypropylene composites. *Polym Compos*. 2001;22:506–17.
- Lonkar SP, Singh RP. Isothermal crystallization and melting behavior of polypropylene/layered double hydroxide nanocomposites. *Thermochim Acta*. 2009;491:63–70.
- Xu W, Liang G, Zhai H, Tang S, Hang G, Pan W-P. Preparation and crystallization behaviour of PP/PP-g-MAH/Org-MMT nanocomposite. *Eur Polym J*. 2003;39:1467–74.
- Papageorgiou GZ, Achilias DS, Bikaris DN, Karayannidis GP. Crystallization kinetics and nucleation activity of filler in polypropylene/surface-treated SiO₂ nanocomposites. *Thermochim Acta*. 2005;427:117–28.
- Du M, Guo B, Wan J, Zou Q, Jia D. Effects of halloysite nanotubes on kinetics and activation energy of non-isothermal crystallization of polypropylene. *J Polym Res*. 2010;17:109–18.
- Avrami M. Kinetics of phase change. I. General theory. *J Chem Phys*. 1939;7:1103–12.
- Avrami M. Kinetics of phase change. II. Transformation-time relations for random distribution of nuclei. *J Chem Phys*. 1940;8:212–24.
- Avrami M. Kinetics of phase change. III. Granulation, phase change, and microstructure. *J Chem Phys*. 1941;9:177–84.
- Lauritzen JL, Hoffman JD. Extension of theory of growth of chain-folded polymer crystals to large under coolings. *J Appl Phys*. 1973;44:4340–52.
- Hoffman JD, Miller RL. Kinetic of crystallization from the melt and chain folding in polyethylene fractions revisited: theory and experiment. *Polymer*. 1997;38:3151–212.
- Huo H, Meng YE, Li HF, Jiang SC, An LJ. Influence of shear on polypropylene crystallization kinetics. *Eur Phys J E*. 2004;15:167–75.
- Chan TW, Isayev AI. Quiescent polymer crystallization: modeling and measurements. *Polym Eng Sci*. 1994;34:461–71.
- Sorrentino L, Iannace S, Maio ED, Acierno D. Isothermal crystallization kinetics of chain-extended PET. *J Polym Sci Part B Polym Phys*. 2005;43:1966–72.
- Papageorgiou GZ, Achilias DS, Bikaris DN. Macromol. Crystallization kinetics of biodegradable poly(butylene succinate)

- under isothermal and non-isothermal conditions. *Macromol Chem Phys.* 2007;208:1250–64.
35. Varga J. Crystallization, melting and supermolecular structure of isotactic polypropylene. In: Karger-Kocsis J, editor. Polypropylene: structure, blends and composites. Vol. I. Structure and morphology. London: Chapman and Hall; 1995. p. 56–115.
 36. Clark EJ, Hoffman JD. Regime-III crystallization in polypropylene. *Macromolecules.* 1984;17:878–85.
 37. Zhang Y-F, Xin Z. Isothermal and nonisothermal crystallization kinetics of isotactic polypropylene nucleated with substituted aromatic heterocyclic phosphate salts. *J Appl Polym Sci.* 2006; 101:3307–16.
 38. Nitta KH, Asuka KZ, Liu BP, Terano M. The effect of the addition of silica particles on linear spherulite growth rate of isotactic polypropylene and its explanation by lamellar cluster model. *Polymer.* 2006;47:6457–63.
 39. Wang K, Wu JS, Zeng HM. Radial growth rate of spherulites in polypropylene barium sulfate composites. *Eur Polym J.* 2003; 39:1647–52.
 40. Menyhárd A, Faludi G, Varga J. β -Crystallisation tendency and structure of polypropylene grafted by maleic anhydride and its blends with isotactic polypropylene. *J Therm Anal Calorim.* 2008;93:937–45.
 41. Wang Y, Shen H, Li G, Mai K. Crystallization and melting behavior of PP/nano-CaCO₃ composites with different interfacial interaction. *J Therm Anal Calorim.* 2010;99:399–407.